Atmospheric Environment 219 (2019) 117013

Contents lists available at ScienceDirect

Atmospheric Environment

journal homepage: http://www.elsevier.com/locate/atmosenv

A fast forecasting method for $PM_{2.5}$ concentrations based on footprint modeling and emission optimization

Mingyuan Yu, Xuhui Cai *, Yu Song, Xuesong Wang

State Key Lab of Environmental Simulation and Pollution Control, College of Environmental Sciences and Engineering, Peking University, Beijing, 100871, China

HIGHLIGHTS

- A fast forecasting method for PM2.5 was developed using a footprint model.
- Promising results were obtained with the primary emission inventory.
- The inverse method improved the forecasts by optimizing the emissions.

ARTICLE INFO

Keywords:
$PM_{2.5}$ forecasting
Footprint model
Emission inventory
Inversion method

ABSTRACT

We propose a method for fast forecasting of $PM_{2.5}$ concentrations in the North China Plain based on footprint (source–receptor relationship) modeling and emission inventory inversion. A backward Lagrangian stochastic particle dispersion model was employed to derive the footprint, using meteorological fields and boundary layer parameters provided by the WRF model. An analytical Bayesian inversion model was used to optimize existing emission inventories using long-term, multi-site $PM_{2.5}$ monitoring data. The fast simulation of $PM_{2.5}$ concentrations was based on the optimized inventory and the footprint results. Two-year simulations were carried out for six cities (Baoding, Beijing, Dezhou, Shijiazhuang, Tianjin, and Tangshan), with model establishment and emission inversion in the first year (2015) and test forecasting in the second year (2016). Promising simulation results were obtained even when using the primary emission inventory. For all six cities, the fractions of simulations of measurements within a factor of two ranged from 0.49 to 0.68, and the correlation coefficients ranged from 0.40 to 0.56 in 2015. The model also well reproduced temporal variations in $PM_{2.5}$ concentrations in Beijing during severe haze episodes in the winter of 2015. Great improvement was achieved for the simulations by using the optimized emission inventory. The proportion of samples that met the PM model criteria increased from 88% to 97%, and the proportion that achieved the modeling goal increased from 25% to 44%. This method maintained its high forecasting skill in 2016, with 92% and 46% of samples meeting the PM model criteria and achieving the modeling goal, respectively. However, the corresponding values were86% and 39% if emission optimization was not applied.

1. Introduction

China has been facing serious air pollution problems recently, with the major pollutant in most cities being particulate matter with an aerodynamic diameter $<2.5\,\mu g$ ($PM_{2.5}$) (Song et al., 2017; Wang et al., 2017). The North China Plain (NCP), a densely populated area that surrounds the capital, Beijing, is one of the most polluted regions in China (Ji et al., 2014). The Chinese government has taken aggressive steps to improve air quality, including a series of 5-year plans for emission reductions and stringent environmental protection laws (summarized in Zheng et al., 2018). Recent studies have reported the effectiveness of these regulations. During the period of 2010–2017, significant emission reductions were estimated for sulfur dioxide (SO_2), nitrogen oxides (NO_x), carbon monoxide, PM_{10}, $PM_{2.5}$, black carbon, and organic carbon in China, and these reduction rates have accelerated since 2013 (Liu et al., 2016; Zheng et al., 2018). Wang et al. (2017) estimated that the turning points for national emissions of $PM_{2.5}$, SO_2, and NO_X were 2005, 2006, and 2011, respectively. van der A et al. (2017) estimated that without the air quality regulations, the concentrations of SO_2 and NO_2 would be approximately 2.5 times and 25%

* Corresponding author. College of Environmental Sciences and Engineering, Peking University, Beijing, 100871, China.
E-mail address: xhcai@pku.edu.cn (X. Cai).

https://doi.org/10.1016/j.atmosenv.2019.117013
Received 21 May 2019; Received in revised form 21 August 2019; Accepted 25 September 2019
Available online 6 October 2019
1352-2310/

higher, respectively, compared to the current status. However, even with the improvements, the NCP is still frequently hit by severe haze events in winter.

Timely and accurate air quality forecasting, particularly early warning for severe pollution episodes, is crucial. Deterministic models have been widely applied for this purpose, based on detailed knowledge of source emissions, physical processes, and chemical reactions (Wang et al., 2018). Such models are powerful tools in providing temporally and spatially resolved pollutant concentrations as well as chemical compositions of particulate matter. However, these models go far beyond the scope needed for concentration forecasts of regular air pollutants in a specific city. Additionally, insufficient knowledge of sources and physicochemical processes may cause large biases in forecasted concentrations (Stern et al., 2008) because they are sensitive to various input data and parameterizations. Also, due to the computational consumption, it is difficult to analyze interannual and decadal trends of concentrations. On the other hand, the statistical models are based on the relationships between measured contaminant concentrations and their influencing factors (mainly meteorological variables) and are generally constrained to certain regions and/or occasions (Pérez and Reyes, 2006; Stadlober et al., 2008). Statistical models are not able to explain the physical causes and processes of a pollution event. The reliance on historical data may be a great limitation in some regions. Researchers are committed to offering more efficient forecasting methods and are aiming for improved forecast accuracy or/and providing more physical information.

Day-to-day variations in air quality are largely driven by synoptic and local meteorological conditions, regional transport, and sometimes by secondary formation (which is also related to weather conditions), as there are no large changes in emissions during such short periods (Guo et al., 2014; Zheng et al., 2015). Extreme air pollution events over the NCP are generally determined by meteorological conditions. Zhang et al. (2018) revealed that emission control from 2013 to 2017 had little effect on the number of days with extreme pollution levels, although the peaks of air pollution concentrations have indeed leveled out. Many statistical air quality models attempt to perform forecasting based on more physical criteria. Meteorological indices or metrics of varying complexity have been proposed; for example, air stagnation (Korshover and Angell, 1982; Wang and Angell, 1999) has been identified as the weather condition with poor ventilation and no precipitation to wash out pollutants, usually corresponding to air pollution episodes. The air stagnation index (ASI) and its revision have also recently been adapted to be applicable for China (Huang et al., 2017, 2018; Feng et al., 2018). Air pollution potential (Gross, 1970), another measure of the meteorological conditions relevant to air pollution, highlights the inability of the atmosphere to adequately dilute pollutants. It was originally based on macroscale meteorological phenomena (Holzworth, 1962) and then later developed to be dominated by local and/or regional meteorological parameters based on qualitative or semi-quantitative approaches (Kimoanh et al., 2005). In the ASI and most measures of air pollution potential, local meteorological parameters are employed to represent ventilation, a crucial parameter for air pollution. However, local ventilation only denotes clean air sweeping in to replace polluted air. In reality, an air mass transported upwind may be contaminated at different levels. Therefore, non-local factors such as regional transport and recirculation should also be quantified in the air pollution–meteorology relationship. Attempts to quantify recirculation have been made (Allwine and Whiteman, 1994) and have been implemented in many coastal areas (Levy et al., 2008; Russo et al., 2016). However, almost none of the above-mentioned metrics have demonstrated good co-variation with daily or hourly air pollution concentrations.

A more recent effort was presented by Yu et al. (2019) to improve the meteorological metric to better represent air pollution levels. Based on the concept and method of the concentration footprint (Schmid, 2002; Vesala et al., 2008), Yu et al. (2019) proposed an integrated concentration footprint to represent air pollution potential. The footprint is described as a source–receptor relationship (SRR), representing the relative contribution from each element of the surface emission to the measured concentration. It has also been regarded as a source weight function (Vesala et al., 2008). Independent of the source term, the footprint represents all critical influences acting on the pollution concentration, including the transport, dispersion, and local/upwind accumulation of air pollutants, the effect of mixing layer depth, and their spatio-temporal variations. In principle, the air pollutant concentration can be derived immediately from the footprint, if an emission inventory is given.

The emission source is another major determinant of air pollution. Uncertainties in emissions (Zhao et al., 2011) greatly influence the accuracy of air pollution forecasts. The various existing emission inventories used in chemical transport models (CTMs) can result in 40–70% differences in PM_{10} concentrations, and 16–20% (Zhong et al., 2016) or 30–50% (Ma and van Aardenne, 2004) differences in ozone mixing ratios. Though emissions may not be directly involved in the statistical models, the relationships between air pollution and influential factors can be implicitly tuned by certain emission conditions. For example, Yang et al. (2016) showed that, by combining regular meteorological conditions and emission factors, the forecasting ability of the statistical method was effectively improved. However, emission inventories are not updated in a timely manner due to cost and complexity. To our knowledge, the most recent gridded emission inventory for China is for the year 2014 (Huang et al., 2014). This greatly limits air quality forecasts, particularly in the NCP, where emissions have changed significantly in recent years. Another way to optimize or update emission inventories is the inverse method, a widely employed so-called top-down approach that uses atmospheric measurement data in conjunction with the SRR, or simply, the footprint (Rodgers, 2000; Jacob, 2007). Inverse models have been applied to estimate the emissions or fluxes of greenhouse gases (Kopacz et al., 2009; Stohl et al., 2009), as well as to improve air pollution predictions by optimizing emission inventories or adjusting measurement skills (Koo et al., 2015; Hamer et al., 2015).

In this study, we attempted to develop a fast forecasting method for air pollution, focusing on $PM_{2.5}$, the major pollutant in the NCP. Secondary components, formed through chemical reactions in the atmosphere, have significant contributions to ambient $PM_{2.5}$. In NCP, secondary inorganic ions are dominant components in summer and autumn, and the concentrations of secondary organic carbon in spring and summer are lower than those in autumn and winter (Xie et al., 2019; Zhao et al., 2013). Though there are seasonal variations, the temporal variation patterns of different components are similar in the hourly/daily view (Liu et al., 2019). Besides, the major processes influencing the concentration of $PM_{2.5}$ are linear: advection, diffusion, deposition, and several first-order chemical reactions (Seibert and Frank, 2004). Therefore, we assume that $PM_{2.5}$ concentrations are determined by (or linearly related to) primary emissions. Under this circumstance, the footprint amplifies the influence of the primary emissions on the atmospheric concentration. As a result, the constrained emission inventory may not represent the actual emissions. Here, we aim to obtain a suitable emission inventory (or a pseudo emission inventory) that will allow the footprint model to perform better air pollution simulations, and furthermore, to offer rapid alerts for air pollution events.

First, we used a footprint model and existing emission inventories to establish fast forecasting of $PM_{2.5}$ concentrations for specific sites (cities). Second, we used $PM_{2.5}$ monitoring data and an analytical inversion model to optimize the emission inventories and thereby improve agreement between observed and simulated concentrations. Finally, the method's forecasting skill was examined using monitoring data from another year. The advantages of this method are two-fold: a) the footprint provides a solid physical basis for fast forecasting of pollutant concentrations; and b) inverse modeling provides optimized (or updated) emissions. In addition, the computational efficiency of this method makes it suitable for both quick response modeling and multi-year

Table 1
WRF parameterization schemes.

Physical mechanism	Parameterization scheme
Microphysics	WSM3 scheme
Long wave radiation	RRTM scheme
Short wave radiation	Duhbia scheme
Surface layer	The Monin-Obukhov
Land surface	NOAH
Planetary boundary layer	YSU scheme
Cumulus parameterization	Kain-Fritsch eta scheme

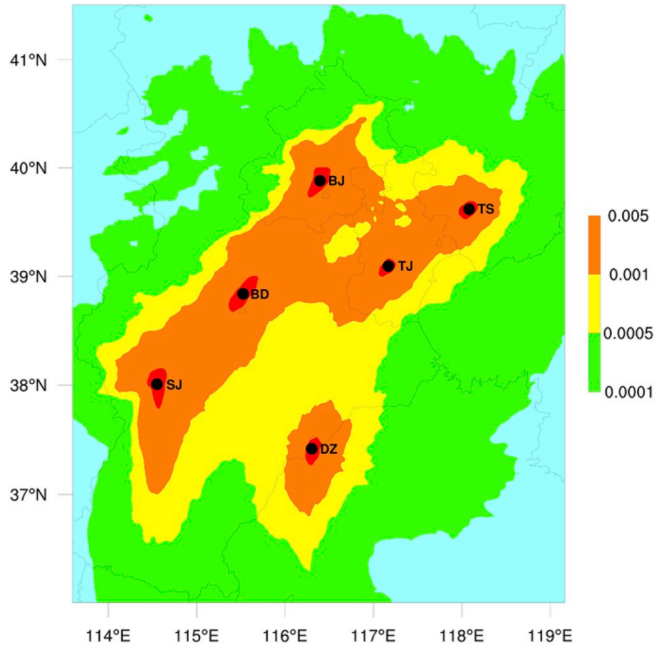

Fig. 1. The source–receptor relationships (SRRs) of six cities in 2015. Unit: 10^{-6}s m^{-3}; BD: Baoding; BJ: Beijing; DZ: Dezhou; SJ: Shijiazhuang; TJ: Tianjin; TS: Tangshan. (color not needed, 1 column)

simulations. This paper is organized as follows. Methods, models, and datasets are introduced in Section 2. The model's ability to predict air pollutant concentrations, especially during severe pollution episodes, and sensitivity tests, are presented in Section 3. Conclusions and discussions are presented in Section 4.

2. Methods and data

2.1. Footprint model and the source–receptor relationship (SRR)

By definition, the concentration footprint, K_{ij}, relates the receptor concentration vector, y_i, to the source vector, x_j, as follows:

$$y_i = \sum_j K_{ij} \cdot x_j. \quad (1)$$

The footprint, K_{ij}, is a linear SRR (or source–receptor matrix, SRM). In reality, the SRM can be linear or nonlinear. The concept and method of the footprint (Schmid, 2002; Vesala et al., 2008) can be utilized because the linear SRM is adopted in this study.

In principle, by using hourly footprints and the emission inventory, air pollution concentrations can be predicted quickly using Eq. (1). In practice, however, Eq. (1) is affected by various factors such as systematic errors caused by WRF and/or footprint models, underestimate in emission inventory, and the secondary transformation of $PM_{2.5}$. The secondary PM fraction in our case is treated as proportional to the primary emissions. It means that the percentage or ratio of secondary $PM_{2.5}$ in the total concentration is assumed a constant. A simplest adjustment to Eq. (1) is to replace K_{ij} with an effective footprint function, i.e., $K'_{ij} = \alpha K_{ij}$, where the coefficient α need to be specified by experience. Based on one-year simulation of 2015, we adopted the coefficient value to be 8 in this study. For simplicity, we keep the form of Eq. (1) unchanged but refer to the footprint K_{ij} as effective footprint, and the same in all relevant formulas hereafter.

Table 2
Locations of concerned cities (receptors in the footprint model).

ID	city	latitude(°N)	longitude(°E)
BJ	Beijing	39.92	116.40
BD	Baoding	38.88	115.49
DZ	Dezhou	37.46	116.30
SJ	Shijiazhuang	38.03	114.49
TJ	Tianjin	39.13	117.21
TS	Tangshan	39.64	118.18

The footprint (or SRM) we used was derived using a Lagrangian particle dispersion model (LPDM) running in backward-in-time mode. The possibility and advantages of calculating a linear SRM with a backward LPDM were demonstrated by Seibert and Frank (2004). LPDM tracks a bunch of passive tracer particles in the turbulent atmosphere. Assuming independent in their motions, the trajectories of these particles are calculated using the mean winds provided by the WRF model and turbulent velocities parameterized in the atmospheric boundary layer. The performance of our LPDM has been thoroughly evaluated under various boundary layer conditions and stabilities for footprint modeling (Cai and Leclerc, 2007; Cai et al., 2008). This model has also been applied to reveal the role of glacier winds in vertical exchange processes over complex mountain terrain (Cai et al., 2007). The details of the model can be found in these references.

The meteorological data used to drive the LPDM were provided by the Weather Research and Forecasting (WRF) model (WRF-ARWv3.6.1; http://www.wrf-model.org/), initialized with the Final Analysis data from the United States National Centers for Environmental Prediction. Two nested domains were used in this study, with horizontal resolutions of 15 km and 5 km, and 28 vertical levels. There was a 12-h spin-up time before the start of each 48-h simulation. The major physics options are summarized in Table 1. The LPDM runs in the WRF's domain 2, which covers the NCP (500 × 600 km) at 2.5 × 2.5-km horizontal resolution, centered on 116.38°E, 39.90°N. Three-dimensional wind fields are used directly in the LPDM. Turbulent variables in the boundary layer are parameterized by hourly values of boundary layer height (z_i), Obukhov length (L), friction velocity (u_*), and surface roughness length (z_0), which are available from the WRF. A set of empirical formulae for turbulent velocity variances and Lagrangian time scale were adopted following Hanna and Sandall (1982) throughout the depth of the boundary layer.

Six representative cities in the NCP were selected; their locations are shown in Fig. 1, and their details are listed in Table 2. Every hour, the footprint was derived for each receptor site by releasing 5000 particles at 10 m above the ground at the site. Each particle was then tracked backward in time for 48 h. The residence times of all particles within a grid with a depth of 400 m above the ground were recorded to obtain the hourly footprint. Fig. 1 shows the study area and the mean footprint in 2015 for all six receptor sites (cities).

2.2. Inversion method

Emission inversion was employed in this study both to optimize and to deal with possible changes in the a priori inventory. The inverted (a posteriori) emissions are derived using an analytic Bayesian inversion method (Rodgers, 2000; Jacob, 2007). The method optimizes the a priori inventory using the observed pollutant concentration and SRM while considering uncertainties for both the a priori inventory and the

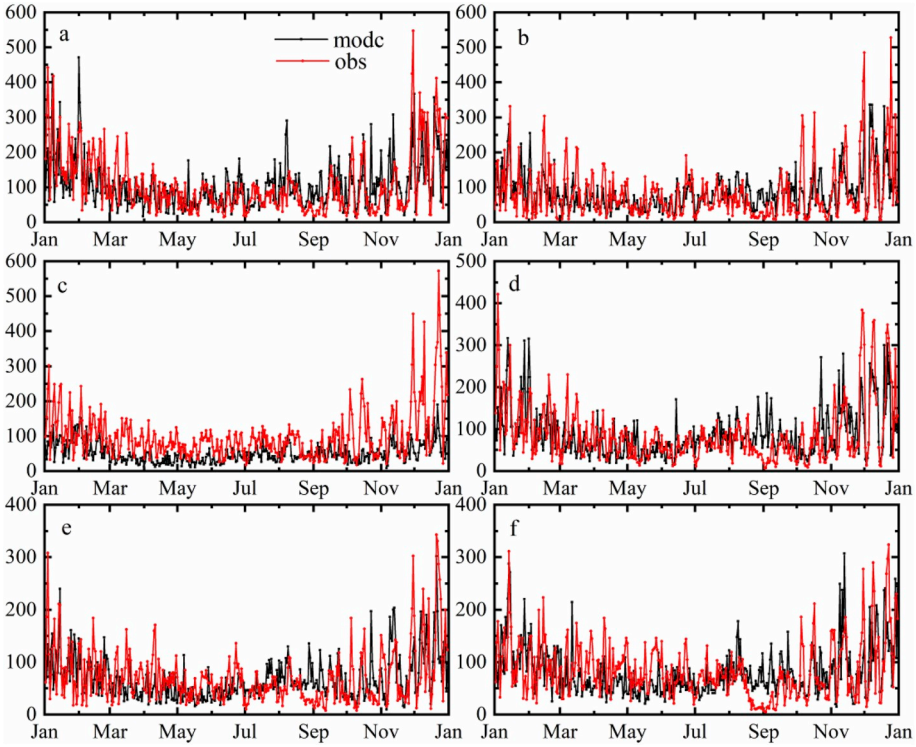

Fig. 2. Day-to-day variations in simulated and observed $PM_{2.5}$ concentrations for six cities in 2015. (a) BD; (b) BJ; (c) DZ; (d) SJ; (e) TJ; (f) TS. Black line (modc): modeled concentrations; red line (obs): observed concentrations. (color should be used, 1.5 columns). (For interpretation of the references to color in this figure legend, the reader is referred to the Web version of this article.)

observations. Following Gaussian error distributions assumed for both the observations and a priori inventory, the purpose of the inversion method is to find the best estimate of x that minimizes the following cost function J:

$$J(x) = (x - x_a)^T S_a^{-1}(x - x_a) + (y - Kx)^T S_\varepsilon^{-1}(y - Kx), \quad (2)$$

where x is the unknown source emission (a posteriori), y is the measurement vector of pollutant concentration, K is the SRM, x_a is the a priori source vector, $y - Kx$ is the difference between the simulated and observed pollutant concentrations, and S_a and S_ε are the error covariance matrices of the a priori emission and the observations, respectively. To minimize $J(x)$ means to solve for $\nabla_x J(x) = 0$. The optimized a posteriori emission vector (x) is given as

$$x = x_a + \left(K^T S_\varepsilon^{-1} K + S_a^{-1}\right)^{-1} K^T S_\varepsilon^{-1}(y - Kx_a), \quad (3)$$

and the a posteriori error covariance $\widehat{S}$ is

$$\widehat{S}^{-1} = K^T S_\varepsilon^{-1} K + S_a^{-1}. \quad (4)$$

The details of the algorithm are described in Rodgers (2000) and Jacob (2007).

The error covariance matrices S_a and S_ε are major parameters in inverse modeling. They can be expressed as $S = diag(\sigma^2)$, assuming there are no correlations between the errors. The uncertainties of the emissions, σ_a, are defined as 100% of the net emissions for all elements. We determined σ_ε to be constant in time for each month, similar to Stohl et al. (2009), calculated as the root mean square error (RMSE) between a primary simulation and observation, averaged for each receptor site. Pre-tests of the model's sensitivity to these two parameters were performed (data not presented here). The chosen parameter set resulted in better simulations of $PM_{2.5}$ air pollution.

In the inverse modeling, the two-dimensional emissions are assumed to be constant for each month. Hourly measurements of $PM_{2.5}$ concentration and the corresponding footprint are employed to constrain the monthly emission. For calculation efficiency, 6×6 grids are aggregated as one element in the inverse modeling.

2.3. Datasets and model evaluation protocols

The routine monitoring data of air pollutant concentrations were downloaded from the Data Center of the Ministry of Ecology and Environment of the People's Republic of China (http://datacenter.mep.gov.cn). Hourly $PM_{2.5}$ measurements for 2015–2016 were used in this study. Meteorological measurements used for model evaluation were obtained from the National Meteorological Information Center (http://data.cma.cn/).

Two sets of emission inventories were used in the simulations to act as the a priori emissions in the inversion method. The first set was produced and provided by Peking University (PKU, http://inventory.pku.edu.cn/). A series of global emission inventories was developed using a bottom-up approach with $0.1^\circ \times 0.1^\circ$ spatial resolution and monthly temporal resolution covering the period from 1960 to 2014. These are the most recent inventories that cover the NCP. Primary $PM_{2.5}$ emissions were used in this study (Huang et al., 2014). The inventory features high sectorial resolution (77 primary sources), with contributions from anthropogenic activities and major natural sources. The second inventory, MIX, was developed by Tsinghua University (http://www.meicmodel.org) for the years 2008 and 2010 over Asia (Li et al., 2017). Monthly gridded emissions were generated for five sectors (power, industry, residential, transportation, and agriculture) at a uniform spatial resolution of $0.25^\circ \times 0.25^\circ$.

To evaluate the model performance, several common statistical metrics were used, including the normalized mean bias (NMB), normalized mean error (NME), RMSE, mean fractional error (MFE), mean fractional bias (MFB), correlation coefficient (R), and the fraction of predictions within a factor of two of observations (FAC2). The definitions and formulations for these metrics can be found in Hanna et al.

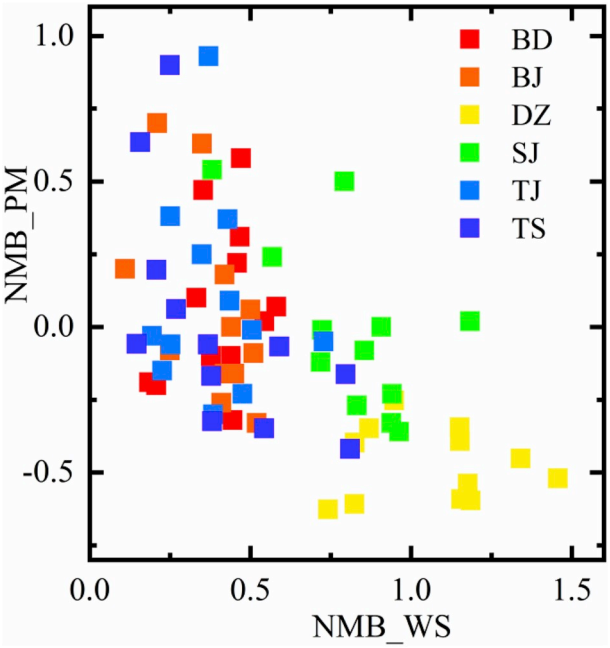

Fig. 3. The relationship between normalized mean biases (NMBs) of $PM_{2.5}$ concentration and wind speed. (color should be used, 1 column). (For interpretation of the references to color in this figure legend, the reader is referred to the Web version of this article.)

(2004) and Zhang et al. (2012). In this study, daily mean values were used in the model evaluations. Boylan and Russell (2006) recommended that a PM model performance is considered to be close to the best (goals) when both the MFE and the MFB are less than or equal to +50% and ±30%, respectively. And the level of model accuracy that is considered to be acceptable (criteria) when both the MFE ≤+75% and MFB ≤±60%.

3. Results

3.1. Basic simulation

Fig. 2 shows the simulated daily mean $PM_{2.5}$ concentrations for 2015 using the footprint model and the PKU 2014 emission inventory. Daily $PM_{2.5}$ measurements are also shown for comparison. For all six cities, the $PM_{2.5}$ concentrations exhibited an annual cycle: high in winter and autumn months (January, February, and October to December), and low in the summer. The simulation results well reproduced this characteristic. Generally, the simulated concentrations were in good agreement with the observations for all cities except Dezhou, where they were underestimations throughout the year. For day-to-day variations, the simulation results successfully depicted most severe winter haze events. These results show that the current modeling method is quite promising.

Detailed analysis of the simulation results in Fig. 2 showed that, for most cities, there were underestimations in spring and winter months and overestimations in summer and autumn months. We attributed the spring discrepancy to sandstorms, which are active during this season in the NCP, with long-term transport being essential (Wang et al., 2015). The summer discrepancy might be caused by rainfalls during the prevailing summer monsoon. Neither the source of the sandstorms nor the effect of wet deposition were included in the current method.

Some discrepancy may also come from the spatio-temporal differences of uncertainty of the meteorology parameters simulated by WRF, especially the wind speeds. Wind speeds in the WRF model grid nearest to the meteorological station were extracted and compared to the corresponding observations. The NMBs of modeled $PM_{2.5}$ concentrations showed a strong negative correlation with the NMBs of simulated wind speeds (Fig. 3). The simulated wind speeds were overestimated by around 10–60% for Baoding, Beijing, Tianjin, and Tangshan, around 70–150% for Dezhou, and in most months for Shijiazhuang, thus leading to discrepancies between the simulated and observed $PM_{2.5}$ concentrations.

The statistical metrics for the $PM_{2.5}$ simulations are listed in Table 3. The primary emissions provide relatively good simulations, with NMBs ranging from −0.05 to 0.02, and FAC2s ranging from 0.60 to 0.68, except for Dezhou, for which both the NMB and FAC2 were 0.49. R-values for all six cities were above 0.4 (0.40–0.56), and NMEs ranged from 0.49 to 0.56. To present the model performance for each month, MFEs (horizontal axis) and MFBs (vertical axis) of daily-averaged $PM_{2.5}$ concentrations for all six cities are drawn in Fig. 4 as the soccer plot (Wang et al., 2018). Based on the recommendation of Boylan and Russell (2006), The inner box represents the particulate matter modeling goal (both the MFE and the MFB are less than or equal to +50% and ±30%, respectively), and the outer box represents the modeling criteria (both the MFE ≤+75% and MFB ≤±60%, respectively). According to Fig. 4a, most months/cities met the criteria, with nine exceptions of 72 samples. Of the 72 samples, about 25% and 88% met the modeling goal and criteria recommended by Boylan and Russell (2006), respectively.

The ability to simulate polluted days is important for a model. There were heavy pollution episodes in autumn and winter in 2015 in the NCP; they have been discussed previously in the literature (Wang et al., 2018; Zhang et al., 2017). We chose the simulation result in Beijing as an example. The time series of observed and simulated $PM_{2.5}$ concentrations are shown in Fig. 5. In general, the simulated day-to-day variations in $PM_{2.5}$ concentrations agreed fairly well with the observations. According to the Technical Regulation on Ambient Air Quality Index (Ministry of Ecology and Environment, 2012), the air quality is classified as polluted when the 24-h mean $PM_{2.5}$ concentration is higher than 115 μg/m^3. Fig. 5 shows that there were 13 and 17 polluted days with $PM_{2.5}$ as the major pollutant in November and December 2015, respectively. Among them, 7 and 14 days, respectively, were detected by the simulation (with an additional 3 days with simulated $PM_{2.5}$ concentrations above 100 μg/m^3). False alarms (over warning) for these months occurred for 1 and 3 days, respectively (including 3 days for which the observations were above 100 μg/m^3). While these results are not perfect, they are satisfactory.

Two periods with underestimations that lasted for more than one day

Table 3
Statistical metrics of the simulations in 2015. "Pri" refers to simulations using the primary PKU 2014 emissions; "Opt" refers to re-simulations using the optimized emissions.

city	RMSE		NME		MFE		MFB		r		FAC2	
	pri	opt	pri	opt	pri	opt	pri	opt	pri	opt	pri	opt
BD	73.2	68.1	0.49	0.45	0.51	0.49	0.07	−0.01	0.56	0.62	0.67	0.72
BJ	64.0	61.7	0.52	0.48	0.54	0.49	0.17	0.09	0.56	0.60	0.66	0.71
DZ	82.5	60.1	0.56	0.42	0.68	0.43	−0.55	−0.06	0.40	0.60	0.49	0.81
SJ	68.2	67.5	0.55	0.53	0.54	0.54	0.09	−0.02	0.47	**0.45**	0.64	0.66
TJ	50.0	47.8	0.53	0.49	0.56	0.52	0.02	**−0.06**	0.46	0.51	0.60	0.69
TS	55.5	53.4	0.51	0.48	0.54	0.52	0.01	0.00	0.42	0.44	0.68	0.70

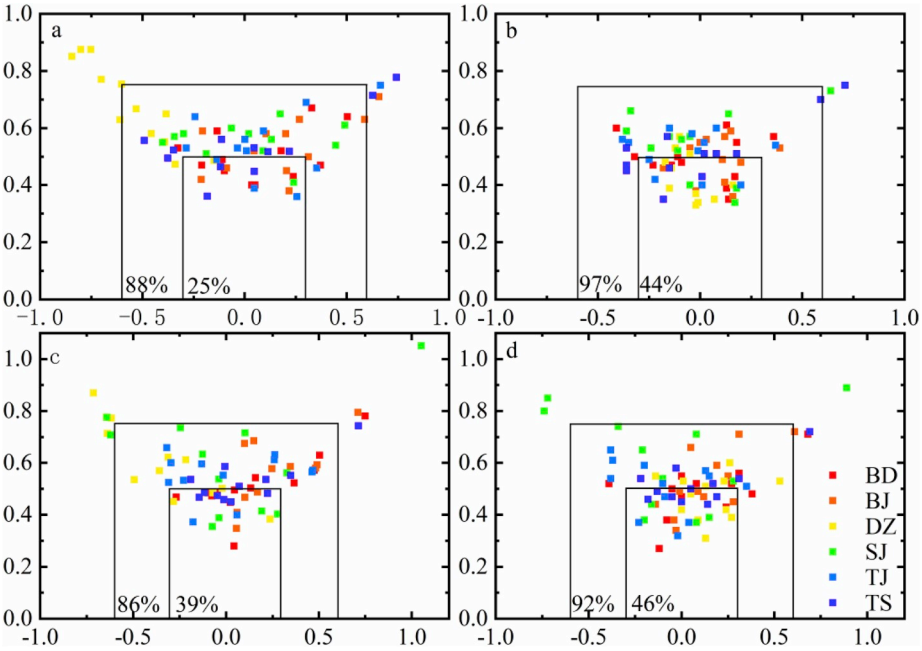

Fig. 4. Soccer plot of daily-averaged $PM_{2.5}$ concentrations for each month in six cities. The inner box represents the particulate matter modeling goal; the outer box represents the modeling criteria. (a) The simulations for 2015 using the primary PKU 2014 emission data; (b) the re-simulations for 2015 using the optimized PKU 2014 emissions; (c) the simulations for 2016 using the primary PKU 2014 emission data; (d) the forecasts for 2016 using the optimized emissions constrained for 2015. (color should be used, 1.5 columns). (For interpretation of the references to color in this figure legend, the reader is referred to the Web version of this article.)

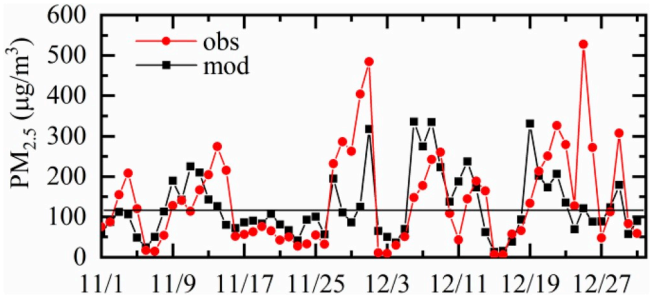

Fig. 5. Measurements and simulations of winter haze in November and December 2015. (color not needed, 1 column)

are obvious in Fig. 5: November 28–30 and December 25–26. The ratios of simulations to observations were lower than 0.5 in these periods. Wang et al. (2018) also reported a failure to simulate the episode during December 25–26 using a three-dimensional CTM with high horizontal resolution. Zhang et al. (2017) found it difficult to reproduce these two episodes using an online-coupled WRF-Chem model. By comparing the model to meteorological observations, Zhang et al. (2017) found that the simulated wind speed was largely overestimated during November 28–30, while during December 25–26, the high relative humidity (>90%) was not reproduced by the WRF. These factors may contribute to the large biases of the $PM_{2.5}$ simulations in contrast to the actual episodes. These factors also exist in the present study.

3.2. Emission inversion and model evaluation

The distributions of $PM_{2.5}$ emissions taken from the PKU 2014 emission inventory and constrained by inverse modeling are shown in Fig. 6a and b. The main features of the distributions are similar. Large emissions are concentrated around major cities in the NCP, including all six cities modeled in this study, as well as Zhangjiakou in the northwest and Jinan in the southeast. The differences between the optimized and the primary emissions are shown in Fig. 6c. The major increases are around Beijing, Tianjin, Tangshan and Dezhou, and the decreases are mainly in the northeast. The significant increases around Dezhou may be a compensation for the system errors cause by the WRF simulation.

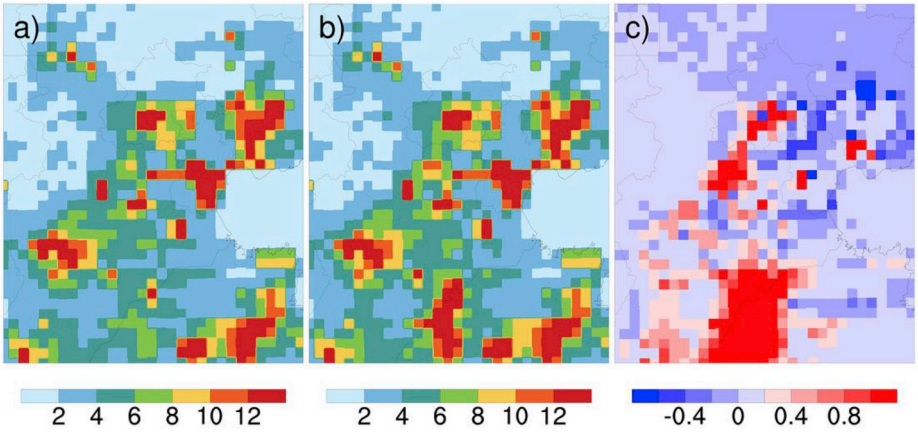

Fig. 6. The distribution of $PM_{2.5}$ emissions. a) The primary PKU 2014 emission inventory; b) The optimized emission based on inverse modeling; c) The differences between the optimized and the primary emissions (optimized - primary); unit: g yr^{-1} m^{-2}. (color should be used, 1.5 columns). (For interpretation of the references to color in this figure legend, the reader is referred to the Web version of this article.)

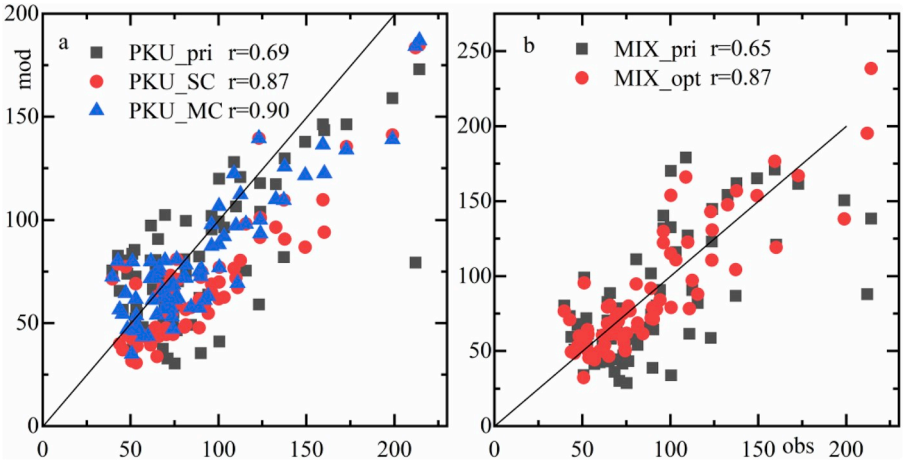

Fig. 7. Comparison of simulated monthly mean $PM_{2.5}$ concentrations with the observations. (a) The emissions from PKU 2014. Black squares: using primary emissions; red circles: using optimized emissions constrained by measurements from single cities (SC); blue triangles: using optimized emissions constrained by measurements from six cities (MC). (b) The emissions from MIX 2010. Black squares: using primary emissions; red circles: using optimized emissions. (color not needed, 1.5 columns). (For interpretation of the references to color in this figure legend, the reader is referred to the Web version of this article.)

Table 4
Statistical metrics of the simulations in 2016. "Pri" refers to simulations using the primary PKU 2014 emissions; "Opt" refers to forecasts using the optimized emissions constrained for 2015.

city	RMSE		NME		MFE		MFB		r		FAC2	
	pri	opt	pri	opt	pri	opt	pri	opt	pri	opt	pri	opt
BD	63.8	59.3	0.51	0.47	0.52	0.50	0.17	0.11	0.51	0.56	0.65	0.70
BJ	56.8	54.8	0.54	0.50	0.56	0.53	0.23	0.14	0.54	0.57	0.63	0.67
DZ	60.8	54.0	0.53	0.49	0.61	0.47	−0.34	0.15	0.28	0.45	0.57	0.74
SJ	92.9	**95.7**	0.59	0.59	0.61	0.61	0.01	**−0.08**	0.39	**0.36**	0.58	**0.57**
TJ	53.6	52.4	0.54	0.50	0.55	0.51	0.00	**−0.09**	0.44	0.49	0.64	0.68
TS	56.1	55.4	0.54	0.53	0.52	0.52	0.09	0.08	0.37	0.38	0.68	0.69

After the inversion, the optimized emissions provided better simulations for all six cities. The RMSEs decreased from 50.0–82.5 to 47.8–68.1, and the NMEs decreased to 0.42–0.53. R-values increased to 0.44–0.62, and FAC2s increased to 0.66–0.81. The improvements were especially prominent in Dezhou, where the NME decreased from 0.56 to 0.42, and the FAC2 increased from 0.49 to 0.81. Comparisons of monthly mean measurements and simulated pollutant concentrations with the primary and optimized emissions are presented in Fig. 7a. The optimized emissions improved the model's simulation skills significantly, with the R-value increasing from 0.69 to 0.90. With the optimized emissions, the percentage of samples that met the modeling goal and criteria increased from 25% to 44% and from 88% to 97%, respectively (Fig. 4b). Only Shijiazhuang and Tangshan in September failed to meet the criteria.

As elucidated above, the $PM_{2.5}$ underestimation in Dezhou was mostly caused by the overestimation of wind speed. The inversion method narrows the differences between the measurements and simulations by using the adjusted or optimized emissions. In summary, while the optimized emissions may not represent reality, the inversion method greatly improves the model's ability to reproduce $PM_{2.5}$ concentrations.

3.3. $PM_{2.5}$ forecast for 2016

$PM_{2.5}$ concentrations in 2016 were forecasted using the optimized emission inventory for 2015. To compare the efficiency of the emission inversion, the model was also run with the primary emissions. The two sets of modeling results were contrasted with the observations in 2016; the statistical metrics are listed in Table 4. The simulations with the PKU 2014 primary emissions were degraded in 2016 compared to those in 2015, with R-values of 0.37–0.54 (0.28 for Dezhou) and NMEs ranging from 0.51 to 0.59, although the FAC2s were similar to those in 2015, ranging from 0.57 to 0.68. Given that the emission inventory was for the year 2014, the degradation might be foreseeable when considering the year-to-year emission changes in the NCP.

The forecasts using the optimized emissions were improved for all cities except Shijiazhuang. The RMSEs decreased from 53.6–63.8 to 52.4–59.3 (from 92.9 to 95.7 in Shijiazhuang), NMEs decreased from 0.51–0.54 to 0.47–0.53 (no change in Shijiazhuang: 0.59), R-values increased from 0.28–0.54 to 0.38–0.57 (0.39–0.36 in Shijiazhuang), and FAC2s increased from 0.57–0.68 to 0.67–0.74 (0.58–0.57 in Shijiazhuang). Comparing the observations with the monthly mean concentrations simulated using the primary and optimized emissions, the correlation coefficients were 0.66 and 0.72, respectively (figure not shown). The proportion of months that achieved the simulation goal increased from 39% to 46%, and the proportion meeting the criteria increased from 86% to 92% (Fig. 4c and d).

Table 5
Statistical metrics of the simulations using MIX 2010 emissions in 2015.

city	ave_obs	ave_mod	NMB	RMSE	NME	MFE	MFB	r	FAC2
BD	106.3	80.0	−0.25	71.42	0.46	0.50	0.19	0.62	0.69
BJ	83.5	91.2	0.09	70.55	0.57	0.54	−0.16	0.57	0.66
DZ	100.6	50.9	−0.49	81.33	0.56	0.69	0.58	0.45	0.47
SJ	87.1	94.3	0.08	69.18	0.55	0.53	−0.13	0.51	0.66
TJ	70.7	75.3	0.07	53.57	0.56	0.55	−0.07	0.51	0.65
TS	84.5	103.3	0.22	65.00	0.57	0.53	−0.23	0.46	0.67

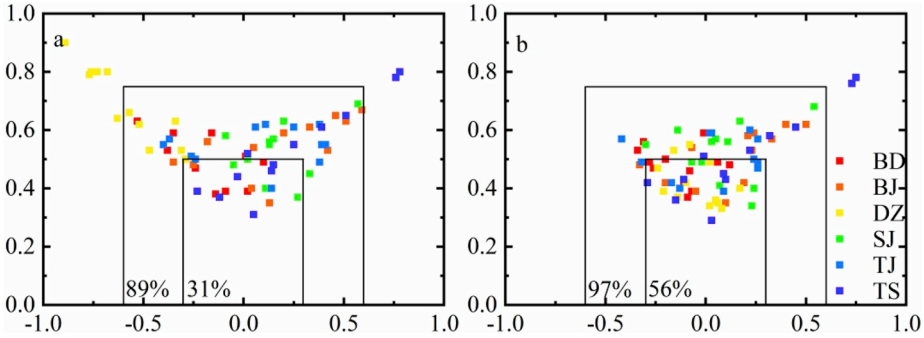

Fig. 8. Soccer plot of daily averaged $PM_{2.5}$ concentrations for each month in six cities. (a) The simulations for 2015 using the primary MIX 2010 emission inventory. (b) The re-simulations for 2015 using the optimized MIX 2010 emissions. (color should be used, 1.5 columns). (For interpretation of the references to color in this figure legend, the reader is referred to the Web version of this article.)

3.4. Sensitivity tests

3.4.1. Influence of the number of cities to be inversed

In previous sections, we use multiple cities for each month in the inverse modeling. This is practical for a region with multiple measurement sites. However, there are occasions when only one site (city) is of concern. Here, we discuss the differences caused by the number of cities used in this method. We operated the inversion model for each city for 12 months in 2015 to obtain six sets of optimized emissions and then calculated the pollutant concentration for each city using the respective set of optimized emissions (noted as SC; the corresponding inversion for multiple cities in Section 3.2 is noted as MC).

For monthly mean concentrations (Fig. 7a), the SCs were mostly underestimated, and the R-value obtained using SCs decreased slightly compared to that for the MC (from 0.90 to 0.87). The FAC2s calculated using the MC were higher than those calculated using SCs for most months in all cities; there were almost no differences in monthly RMSEs between the MC and SCs. It can be concluded that using multiple receptors in the inverse modeling of emissions can provide better simulations. By using more cities, the footprints used in the inversion might overlap or cover more areas in the simulation domain, providing better spatial representativeness, and leading to better-constrained a posteriori emissions.

3.4.2. Influence of the a priori emissions

To test the forecast ability of the model using different primary emissions, the simulations and analysis were performed again using the MIX 2010 emissions. With the primary emissions, MIX 2010 performed worse for RMSEs and NMEs, but better for R-values and FAC2s (Table 5) when compared to the simulations using PKU 2014. The monthly mean simulations using MIX 2010 were less well correlated with observations than were simulations using PKU 2014, as shown in Fig. 7b. However, more simulated months achieved the model goal using MIX 2010 (31%) than when using PKU 2014 (25%) (Fig. 8a). Thus, neither of these two primary emission inventories had a clear advantage over the other.

After the inversion, the re-simulations using optimized MIX 2010 emissions were similar to those using optimized PKU 2014 emissions. The RMSEs and R-values for MIX 2010 were slightly higher than those for PKU 2014. In the MFE–MFB plot for MIX 2010 (Figs. 8b), 97% of months met the model criteria, which was the same as with PKU 2014, while 56% of months achieved the model goal, which was higher than with PKU 2014. The correlation coefficient between the monthly mean measurements and simulations was 0.87 for MIX 2010, which was slightly lower than that for PKU 2014.

Overall, the two sets of primary emissions were optimized by the inversion method, and either might have a slight advantage over the other, depending on the evaluation metrics. This suggests that inversion is capable of optimizing emissions for forecasting even when a relatively coarse emission source is supplied as the a priori. Therefore, this method has the potential to be applied for air quality forecasting in situations when the bottom-up emission inventories are not regularly updated.

4. Conclusions

We proposed a fast forecasting method for $PM_{2.5}$ concentrations based on a footprint model and an emission inversion model, which provide the SRR and optimized emissions, respectively. Two-year $PM_{2.5}$ concentration simulations were carried out for six major cities (Baoding, Beijing, Dezhou, Shijiazhuang, Tianjin, and Tangshan) throughout the NCP, with model establishment, evaluation, and emission inversion in the first year and forecasting in the second year. Observational $PM_{2.5}$ data from these cities were used in the model evaluation and emission inversion.

Using the PKU 2014 emission inventories and footprint results, the 2015 day-to-day variations in $PM_{2.5}$ concentrations were reproduced, and severe winter haze events were detected. The correlation coefficients between the simulations and observations for the six cities ranged from 0.40 to 0.56, and the FAC2s ranged from 0.49 to 0.68. Based on the monthly MFEs and MFBs, 88% of samples met the PM model criteria, and 25% achieved the modeling goal. The model also successfully detected 21 of 30 extremely polluted days in the last 2 months of 2015, when severe air pollution episodes occurred. With the optimized emissions, the simulations for all six cities were greatly improved. The FAC2s increased to 0.66–0.81, and the percentages of samples that met the model criteria and goal increased to 97% and 44%, respectively.

The test forecasting for 2016 also showed good performance, with 46% and 92% of samples meeting the criteria and achieving the modeling goal, respectively, based on the monthly MFE and MFB standards. Emission inversion played an important role in the forecasting, as the corresponding percentages were only 39% and 86% when the primary PKU 2014 emissions were applied for 2016.

Further analysis showed that this method was robust and relatively insensitive to the initial emission inventory, but using multiple sites when applying the source inversion provided better simulation results.

In conclusion, the method presented in this paper is physically solid, since both emissions and meteorological influences, the most important factors or variables for air pollution, are properly considered. An inversion model and observational concentration data were used to update and optimize the emission inventory, providing additional improvement of the forecast. This method is also computationally efficient for forecasting air pollution concentrations for single or multiple cities in cases of both short-term and long-term applications, for example, regulatory day-to-day forecasting or research on inter-annual air pollution trends. However, this method cannot provide detailed concentration fields in the research domain. This is the major limitation of this method in comparison to CTMs. The chemical and removal processes of air pollutants are not presently included. Incorporating first-

order chemical reactions into this method may further improve its forecasting performance, and this is a possible future direction. However, a more detailed discussion of uncertainties caused by meteorology and chemistry/removal may help the inversion method to provide a more reliable updated emission inventory in a region, which could be another potential application of this method.

Declaration of competing interest

The authors declare that they have no known competing financial interests or personal relationships that could have appeared to influence the work reported in this paper.

Acknowledgments

This work was supported by Ministry of Finance (DQGG0106-01); National Science and Technology Infrastructure Program (2014BAC06B02) and National Natural Science Foundation of China (41575007, 91544216).

Appendix A. Supplementary data

Supplementary data to this article can be found online at https://doi.org/10.1016/j.atmosenv.2019.117013.

References

Allwine, K.J., Whiteman, C.D., 1994. Single-station integral measures of atmospheric stagnation, recirculation and ventilation. Atmos. Environ. 28, 713–721.
Boylan, J.W., Russell, A.G., 2006. PM and light extinction model performance metrics, goals, and criteria for three-dimensional air quality models. Atmos. Environ. 40, 4946–4959.
Cai, X., Leclerc, M.Y., 2007. Forward-in-time and backward-in-time dispersion in the convective boundary layer: the concentration footprint. Boundary-Layer Meteorol. 123, 201–218.
Cai, X., Peng, G., Guo, X., Leclerc, M.Y., 2008. Evaluation of backward and forward Lagrangian footprint models in the surface layer. Theor. Appl. Climatol. 93, 207–223.
Cai, X., Song, Y., Zhu, T., Lin, W., Kang, L., 2007. Glacier winds in the Rongbuk Valley, north of Mount Everest: 2. Their role in vertical exchange processes. J. Geophys. Res. Atmos. 112.
Feng, J., Quan, J., Liao, H., Li, Y., Zhao, X., 2018. An air stagnation index to qualify extreme haze events in northern China. J. Atmos. Sci. 75, 3489–3505.
Gross, E., 1970. The National Air Pollution Potential Forecast Program. National Meteorological Center, Washington DC.
Guo, S., Hu, M., Zamora, M.L., Peng, J.F., Shang, D.J., Zheng, J., Du, Z.F., Wu, Z., Shao, M., Zeng, L.M., Molina, M.J., Zhang, R.Y., 2014. Elucidating severe urban haze formation in China. Proc. Natl. Acad. Sci. U.S.A. 111, 17373–17378.
Hamer, P.D., Bowman, K.W., Henze, D.K., Attié, J.L., Marécal, V., 2015. The impact of observing characteristics on the ability to predict ozone under varying polluted photochemical regimes. Atmos. Chem. Phys. 15, 10645–10667.
Hanna, O.T., Sandall, O.C., 1982. Turbulent heat transfer in a circular tube with viscous dissipation. Chem. Eng. Commun. 18, 163–172.
Hanna, S.R., Hansen, O.R., Dharmavaram, S., 2004. FLACS CFD air quality model performance evaluation with Kit Fox, MUST, Prairie Grass, and EMU observations. Atmos. Environ. 38, 4675–4687.
Holzworth, G.C., 1962. A study of air pollution potential for the western United States. J. Appl. Meteorol. 1, 366–382.
Huang, Q., Cai, X., Song, Y., Zhu, T., 2017. Air stagnation in China (1985–2014): climatological mean features and trends. Atmos. Chem. Phys. 17, 7793–7805.
Huang, Q., Cai, X., Wang, J., Song, Y., Zhu, T., 2018. Climatological study of the Boundary-layer air Stagnation Index for China and its relationship with air pollution. Atmos. Chem. Phys. 18, 7573–7593.
Huang, Y., Shen, H., Chen, H., Wang, R., Zhang, Y., Su, S., Chen, Y., Lin, N., Zhuo, S., Zhong, Q., Wang, X., Liu, J., Li, B., Liu, W., Tao, S., 2014. Quantification of global primary emissions of PM2.5, PM10, and TSP from combustion and industrial process sources. Environ. Sci. Technol. 48, 13834–13843.
Jacob, D.J., 2007. Lectures on Inverse Modeling. Harvard University.
Ji, D., Li, L., Wang, Y., Zhang, J., Cheng, M., Sun, Y., Liu, Z., Wang, L., Tang, G., Hu, B., Chao, N., Wen, T., Miao, H., 2014. The heaviest particulate air-pollution episodes occurred in northern China in January, 2013: insights gained from observation. Atmos. Environ. 92, 546–556.
Kimoanh, N., Chutimon, P., Ekbordin, W., Supat, W., 2005. Meteorological pattern classification and application for forecasting air pollution episode potential in a mountain-valley area. Atmos. Environ. 39, 1211–1225.
Koo, Y.-S., Choi, D.-R., Kwon, H.-Y., Jang, Y.-K., Han, J.-S., 2015. Improvement of PM10 prediction in East Asia using inverse modeling. Atmos. Environ. 106, 318–328.
Kopacz, M., Jacob, D.J., Henze, D.K., Heald, C.L., Streets, D.G., Zhang, Q., 2009. Comparison of adjoint and analytical Bayesian inversion methods for constraining Asian sources of carbon monoxide using satellite (MOPITT) measurements of CO columns. J. Geophys. Res. 114.
Korshover, J., Angell, J.K., 1982. A review of air-stagnation cases in the eastern United States during 1981— annual summary. Mon. Weather Rev. 110, 1515–1518.
Levy, I., Dayan, U., Mahrer, Y., 2008. A five-year study of coastal recirculation and its effect on air pollutants over the East Mediterranean region. J. Geophys. Res. 113.
Li, M., Zhang, Q., Kurokawa, J.-i., Woo, J.-H., He, K., Lu, Z., Ohara, T., Song, Y., Streets, D.G., Carmichael, G.R., Cheng, Y., Hong, C., Huo, H., Jiang, X., Kang, S., Liu, F., Su, H., Zheng, B., 2017. MIX: a mosaic Asian anthropogenic emission inventory under the international collaboration framework of the MICS-Asia and HTAP. Atmos. Chem. Phys. 17, 935–963.
Liu, F., Zhang, Q., van der A, R.J., Zheng, B., Tong, D., Yan, L., Zheng, Y., He, K., 2016. Recent reduction in NO x emissions over China: synthesis of satellite observations and emission inventories. Environ. Res. Lett. 11, 114002.
Liu, Y., Zheng, M., Yu, M., Cai, X., Du, H., Li, J., Zhou, T., Yan, C., Wang, X., Shi, Z., Harrison, R.M., Zhang, Q., He, K., 2019. High-time-resolution source apportionment of PM2.5 in Beijing with multiple models. Atmos. Chem. Phys. 19, 6595–6609.
Ma, J., van Aardenne, J.A., 2004. Impact of different emission inventories on simulated tropospheric ozone over China: a regional chemical transport model evaluation. Atmos. Chem. Phys. 4, 877–887.
Ministry of Ecology and Environment, 2012. In: Ambient Air Quality Standard (GB3095-2012). Ministry of Ecology and Environment, Beijing, China.
Pérez, P., Reyes, J., 2006. An integrated neural network model for PM10 forecasting. Atmos. Environ. 40, 2845–2851.
Rodgers, 2000. Inverse Methods for Atmospheric Sounding: Theory and Practice. World Scientific Publishing Co. Pte. Ltd. (Chapter 2).
Russo, A., Gouveia, C., Levy, I., Dayan, U., Jerez, S., Mendes, M., Trigo, R., 2016. Coastal recirculation potential affecting air pollutants in Portugal: the role of circulation weather types. Atmos. Environ. 135, 9–19.
Schmid, H.P., 2002. Footprint modeling for vegetation atmosphere exchange studies: a review and perspective. Agric. For. Meteorol. 113, 159–183.
Seibert, P., Frank, A., 2004. Source-receptor matrix calculation with a Lagrangian particle dispersion model in backward mode. Atmos. Chem. Phys. 4, 51–63.
Song, C., Wu, L., Xie, Y., He, J., Chen, X., Wang, T., Lin, Y., Jin, T., Wang, A., Liu, Y., Dai, Q., Liu, B., Wang, Y.N., Mao, H., 2017. Air pollution in China: status and spatiotemporal variations. Environ. Pollut. 227, 334–347.
Stadlober, E., Hörmann, S., Pfeiler, B., 2008. Quality and performance of a PM10 daily forecasting model. Atmos. Environ. 42, 1098–1109.
Stern, R., Builtjes, P., Schaap, M., Timmermans, R., Vautard, R., Hodzic, A., Memmesheimer, M., Feldmann, H., Renner, E., Wolke, R., 2008. A model inter-comparison study focussing on episodes with elevated PM10 concentrations. Atmos. Environ. 42, 4567–4588.
Stohl, A., Seibert, P., Arduini, J., Eckhardt, S., Fraser, P., Greally, B., Lunder, C., Maione, M., Mühle, J., O'doherty, S., 2009. An analytical inversion method for determining regional and global emissions of greenhouse gases: sensitivity studies and application to halocarbons. Atmos. Chem. Phys. 9, 1597–1620.
van der A, R.J., Mijling, B., Ding, J., Koukouli, M.E., Liu, F., Li, Q., Mao, H., Theys, N., 2017. Cleaning up the air: effectiveness of air quality policy for SO_2 and NO_x emissions in China. Atmos. Chem. Phys. 17, 1775–1789.
Vesala, T., Kljun, N., Rannik, Ü., Rinne, J., Sogachev, A., Markkanen, T., Sabelfeld, K., Foken, T., Leclerc, M.Y., 2008. Flux and concentration footprint modelling: state of the art. Environ. Pollut. 152, 653–666.
Wang, J., Zhao, B., Wang, S., Yang, F., Xing, J., Morawska, L., Ding, A., Kulmala, M., Kerminen, V.M., Kujansuu, J., Wang, Z., Ding, D., Zhang, X., Wang, H., Tian, M., Petaja, T., Jiang, J., Hao, J., 2017. Particulate matter pollution over China and the effects of control policies. Sci. Total Environ. 584–585, 426–447.
Wang, J.X.L., Angell, J.K., 1999. Air Stagnation Climatology for the United States. NOAA/Air Resour Lab ATLAS, p. 1.
Wang, L., Liu, Z., Sun, Y., Ji, D., Wang, Y., 2015. Long-range transport and regional sources of $PM_{2.5}$ in Beijing based on long-term observations from 2005 to 2010. Atmos. Res. 157, 37–48.
Wang, Y., Chen, H., Wu, Q., Chen, X., Wang, H., Gbaguidi, A., Wang, W., Wang, Z., 2018. Three-year, 5 km resolution China $PM_{2.5}$ simulation: model performance evaluation. Atmos. Res. 207, 1–13.
Xie, Y., Liu, Z., Wen, T., Huang, X., Liu, J., Tang, G., Yang, Y., Li, X., Shen, R., Hu, B., Wang, Y., 2019. Characteristics of chemical composition and seasonal variations of $PM_{2.5}$ in Shijiazhuang, China: impact of primary emissions and secondary formation. Sci. Total Environ. 677, 215–229.
Yang, Y.Q., Wang, J.Z., Gong, S.L., Zhang, X.Y., Wang, H., Wang, Y.Q., Wang, J., Li, D., Guo, J.P., 2016. Plam – a meteorological pollution index for air quality and its applications in fog-haze forecasts in North China. Atmos. Chem. Phys. 16, 1353–1364.
Zhang, Q., Ma, Q., Zhao, B., Liu, X., Wang, Y., Jia, B., Zhang, X., 2018. Winter haze over north China plain from 2009 to 2016: influence of emission and meteorology. Environ. Pollut. 242, 1308–1318.
Yu, M., Cai, X., Xu, C., Song, Y., 2019. A climatological study of air pollution potential in China. Theor. Appl. Climatol. 136, 627–638.
Zhang, Y., Bocquet, M., Mallet, V., Seigneur, C., Baklanov, A., 2012. Real-time air quality forecasting, part I: history, techniques, and current status. Atmos. Environ. 60, 632–655.
Zhang, Z.Y., Gong, D.Y., Mao, R., Kim, S.J., Xu, J., Zhao, X.J., Ma, Z.Q., 2017. Cause and predictability for the severe haze pollution in downtown Beijing in November-December 2015. Sci. Total Environ. 592, 627–638.

Zhao, P.S., Dong, F., He, D., Zhao, X.J., Zhang, X.L., Zhang, W.Z., Yao, Q., Liu, H.Y., 2013. Characteristics of concentrations and chemical compositions for $PM_{2.5}$ in the region of Beijing, Tianjin, and Hebei, China. Atmos. Chem. Phys. 13, 4631–4644.
Zhao, Y., Nielsen, C.P., Lei, Y., McElroy, M.B., Hao, J., 2011. Quantifying the uncertainties of a bottom-up emission inventory of anthropogenic atmospheric pollutants in China. Atmos. Chem. Phys. 11, 2295–2308.
Zheng, B., Tong, D., Li, M., Liu, F., Hong, C., Geng, G., Li, H., Li, X., Peng, L., Qi, J., Yan, L., Zhang, Y., Zhao, H., Zheng, Y., He, K., Zhang, Q., 2018. Trends in China's anthropogenic emissions since 2010 as the consequence of clean air actions. Atmos. Chem. Phys. 18, 14095–14111.
Zheng, G.J., Duan, F.K., Su, H., Ma, Y.L., Cheng, Y., Zheng, B., Zhang, Q., Huang, T., Kimoto, T., Chang, D., Poschl, U., Cheng, Y.F., He, K.B., 2015. Exploring the severe winter haze in Beijing: the impact of synoptic weather, regional transport and heterogeneous reactions. Atmos. Chem. Phys. 15, 2969–2983.
Zhong, M., Saikawa, E., Liu, Y., Naik, V., Horowitz, L.W., Takigawa, M., Zhao, Y., Lin, N.-H., Stone, E.A., 2016. Air quality modeling with WRF-Chem v3.5 in East Asia: sensitivity to emissions and evaluation of simulated air quality. Geosci. Model Dev. (GMD) 9, 1201–1218.